Low Temperature Physics/Fizika Nizkikh Temperatur, 2015, v. 41, No. 4, pp. 381–388

Propagation of acoustic edge waves in graphene under quantum Hall effect

A. Vikström

Department of Applied Physics, Chalmers University of Technology, Kemigården 1, 412 96 Göteborg, Sweden
E-mail: anton.vikstrom@chalmers.se

Received September 23, 2014, published online February 23, 2015

We consider a graphene sheet with a zigzag edge subject to a perpendicular magnetic field and investigate the propagation of in-plane acoustic edge waves. In particular it is shown that propagation is significantly blocked for certain frequencies defined by the resonant absorption due to electronic-acoustic interaction. We study absorption of acoustic energy as a function of magnetic field and find that, for a finite gate voltage and fixed acoustic frequency, tuning the magnetic field may bring the system through a number of electronic resonances. We suggest that the strong interaction between the acoustic and electronic edge states in graphene may generate significant nonlinear effects leading to the existence of acoustic solitons in such systems.

PACS: **43.35.+d** Ultrasonics, quantum acoustics, and physical effects of sound;
81.05.ue Graphene;
73.43.–f Quantum Hall effects.

Keywords: graphene, quantum Hall effect, strain, edge waves, electron-strain interaction.

The discovery of graphene [1], an ultra-pure 2D crystal membrane of remarkable promise [2], has in just the past few years led to the rapid growth of a new field of research, uniting and challenging scientists from research backgrounds as diverse as the capabilities of the material itself. In addition to its astounding material properties, the very existence of a true 2D crystal both requires and inspires new ways of thinking.

It is well known that a 3D continuous medium supports acoustic waves localized to the surface [3]. Such surface waves have been used to probe the electronic properties of samples [4], e.g., the fractional quantum Hall effect of 2D electron gasses in semiconductor heterostructures [5,6], topological insulators [7,8] and, more recently, graphene [9]. In past schemes the surface wave direction of localization was normal to the 2D electron gas plane so that the electrons experienced no localization of acoustic energy. However, the isolation of single-layer graphene [1], a flexible 2D membrane, suggests the existence of acoustic edge waves, a 2D analog of the 3D surface waves. Recent studies have shown such edge-localized vibrational motion in graphene to consist of both in-plane and flexural modes, both decaying into the 2D "bulk" [10]. At the same time, a magnetic field applied perpendicularly to the sheet would induce current-carrying electronic states localized to the same graphene edge on the order of the magnetic length, $l_B = \sqrt{\hbar/|eB|} \approx 26\ \text{nm}/\sqrt{B\,[\text{T}]}$ ($B\,[\text{T}]$ is the dimensionless field strength in Tesla) [11–17]. In this paper we investigate the interaction between electronic quantum Hall effect edge states and localized acoustic edge waves, specifically low-amplitude in-plane *Rayleigh waves* [3], while flexural modes will be neglected.

To be concrete, we consider a 2D graphene sheet with a stress-free zigzag edge at $y = 0$, directed along the x axis, see Fig. 1. A transverse magnetic field, $\mathbf{B} = -|B|\mathbf{e}_z$, is

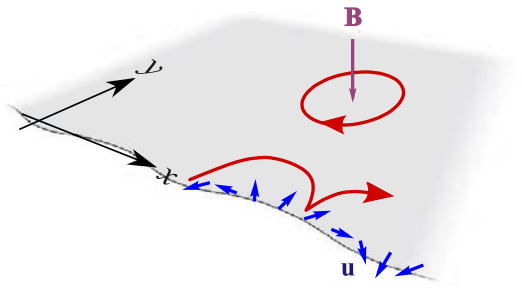

Fig. 1. (Color online) A schematic picture of a continuous (graphene) sheet with an edge along the x axis and an applied perpendicular magnetic field (purple). The electronic states (red) may be either localized Landau orbits in the bulk or dispersive states near the edge. Along the edge there are propagating acoustic (Rayleigh) edge waves given by a 2D displacement field (blue, amplitude exaggerated).

then applied to the sheet ($\mathbf{e}_{x,y,z}$ are unit vectors), bringing the sample into the quantum Hall effect regime. The sheet is treated as a continuous medium and the width of the sample is taken to be large enough for the electronic and acoustic edge states to decay completely across the sample; it is then enough to consider only one edge. The sample length L is assumed to be long enough to allow for acoustic wave propagation in the x direction.

Since the graphene edge, which is normal to $-\mathbf{e}_y$ and located at $y = 0$, is stress-free, the elastic boundary conditions are

$$\sigma_{jy}(x,0) = 0, \quad j = x, y, \tag{1}$$

where $\sigma_{ij}(x,y)$ is the usual 2D stress tensor [3]. Since the Rayleigh waves are pseudo-1D, they can be specified by the wave vector x-component q alone, which will be referred to as the *wave number*. Standard techniques [3] give the two-component displacement field $\mathbf{u}^{(q)}(x,y)$ for an in-plane Rayleigh wave as

$$\mathbf{u}^{(q)}(x,y;t) = 2u_0 \begin{pmatrix} f_x^{(q)}(y)\cos(qx-\omega t) \\ \operatorname{sgn}(q) f_y^{(q)}(y)\sin(qx-\omega t) \end{pmatrix}, \tag{2}$$

where

$$f_x^{(q)}(y) = \mathrm{e}^{-\lambda_l |q| y} - C_x \mathrm{e}^{-\lambda_t |q| y} \tag{3}$$

and

$$f_y^{(q)}(y) = -\lambda_l \mathrm{e}^{-\lambda_l |q| y} + C_y \mathrm{e}^{-\lambda_t |q| y}. \tag{4}$$

The scalar prefactor u_0 is the amplitude, and the dimensionless constants are

$$\lambda_l = 0.81, \quad \lambda_t = 0.46,$$
$$C_x = 0.61, \quad C_y = 1.3, \tag{5}$$

and depend only on the ratio of the transverse and longitudinal sound velocities in graphene, s_t / s_l, or, equivalently, on the Poisson ratio. The sound velocities are taken to be $s_t = 1.4 \cdot 10^4$ m/s and $s_l = 2.1 \cdot 10^4$ m/s [18,19]. The dispersion relation is linear,

$$\omega(q) = s_R |q|, \tag{6}$$

with Rayleigh-wave sound velocity $s_R = 1.2 \cdot 10^4$ m/s.

The electronic subsystem is described by the standard effective-model graphene Hamiltonian

$$\mathbf{H}_{\mathrm{el}} = v^F (\boldsymbol{\sigma}_x \hat{p}_x + \tau \boldsymbol{\sigma}_y \hat{p}_y), \tag{7}$$

where $v^F = 1.0 \cdot 10^6$ m/s is the Fermi velocity of graphene, valley index $\tau = +1$ (-1) for the spectral valley around the K-point (K'-point), the $\boldsymbol{\sigma}_s$ are the sublattice-space Pauli matrices [16,17,20] and the sublattice pseudospinor upon which the Hamiltonian acts is defined by $\psi^\tau(x,y) = (\psi_A^\tau(x,y), \tau\psi_B^\tau(x,y))^T$. The transverse magnetic field is represented by a vector potential in the Landau gauge, $\mathbf{A}_B = (By, 0)^T$, and then included in the Hamiltonian of Eq. (7) through the minimal coupling $\mathbf{p} \to \mathbf{p} + e\mathbf{A}$ (the electron charge is $-e < 0$).

In an infinite bulk system the electronic energies form Landau levels [21–23],

$$E_n = \operatorname{sgn}(n) E_1 \sqrt{|n|}, \quad n = 0, \pm 1, \pm 2, \ldots$$
$$E_1 = \sqrt{2}\hbar v^F l_B^{-1} \propto \sqrt{|B|}, \tag{8}$$

and the electronic wave functions are localized and centered around $y_c = -k l_B^2$ ($k = p_x / \hbar$ being the electron wave number), corresponding to closed Landau orbits, see Fig. 1. This simple picture is modified by the introduction of an edge.

In the considered system the edge at $y = 0$ is a zigzag edge of B-atoms, leading to the electronic boundary condition [24]

$$\psi_A^\tau(x,0) = 0. \tag{9}$$

Since the zigzag boundary condition does not mix valleys the K- and K'-points can be considered separately.

The edge induces a positive (negative) dispersion in the electron-like (hole-like) Landau levels as k increases and the wave function center $y_c \propto -k$ moves toward and over the edge [11], pressing the oscillator wave functions against the edge and turning them into edge-localized current-carrying states. For a classical, intuitive picture of this effect, see Fig. 1.

The dispersion can be calculated by generalizing the Landau-level index n to a *continuous* analogue, $\nu = (E / E_1)^2$, and describing the wave functions with (Whittaker's) parabolic cylinder functions $D_\nu(z)$, which reduce to the wave functions for the bulk electronic states for integer ν but allow for non-integer ν solutions between the bulk Landau levels. The spectrum is then calculated from the boundary condition of Eq. (9) [12–15]. The dimensionless energy $E / E_1 \equiv \tilde{E}$ is schematically plotted against the dimensionless wave number $k l_B \equiv \tilde{k}$ in Fig. 2 for both the K- and K'-points. The energy band stemming from Landau level n will be referred to as "edge band n". When $\tilde{k} = k l_B = 0$, $y_c = 0$ and the wave function is centered on the edge.

As seen in Fig. 2, the zeroth Landau level remains dispersionless for all $\tilde{k}$ in the K'-point spectrum, whereas it is seemingly split in two edge bands, one electron-like and one hole-like, in the K-point spectrum. This can be explained by extra degeneracies introduced by topological edge states; the peculiar nature of the $n = 0$ Landau level have been studied in other papers [14,15,25,26]; for the purpose of this paper the schematic spectra in Fig. 2 will suffice.

The electronic pseudospinor wave functions are given in Appendix A for reference. There, scaled physical coordinates $\tilde{x}(\tilde{y}) \equiv x / l_B (y / l_B)$ are introduced, which will be employed below when considering the absorption.

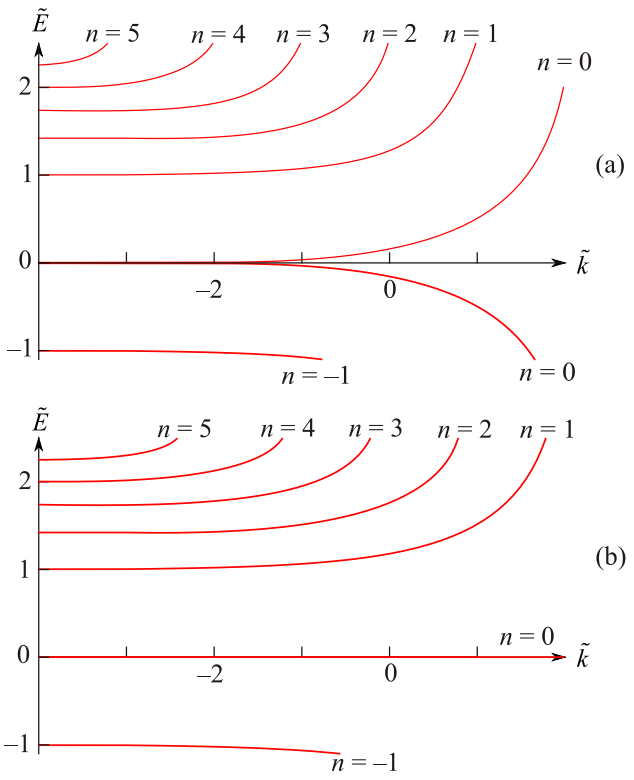

Fig. 2. (Color online) A schematic picture of the electronic spectrum around the points K (a) and K' (b). The scaled energy $\tilde{E} = E / E_1$ is plotted against the scaled wave number $\tilde{k} = kl_B$ (energy bands in red). The leftmost low-$\tilde{k}$ states are bulk states and their spectrum consists of discrete Landau levels. The dispersive states are edge states and here share the label n with their bulk counterparts.

The standard first-order-in-strain Hamiltonian for the electron-strain interaction in graphene is given by [27]

$$\mathbf{H}_{\text{int}}^{\tau}\left(\mathbf{u}(x,y;t)\right) = g_1(u_{xx}+u_{yy})\mathbf{I} + \\ +g_2\left(-\tau(u_{xx}-u_{yy})\boldsymbol{\sigma}_x + 2u_{xy}\boldsymbol{\sigma}_y\right), \qquad (10)$$

where u_{ij} is the standard strain tensor. The diagonal elements are the scalar deformation potential, with coupling constant $g_1 \sim 10$ eV, and the off-diagonal elements are usually imagined as a strain-induced pseudo-vector-potential, and their coupling constant is $g_2 \sim 1$ eV. Since the valley separation is $|\mathbf{K}-\mathbf{K}'| \sim a^{-1}$, with a being the lattice constant, interaction with the acoustic Rayleigh waves will not mix K and K' if the acoustic wave number $q \ll a^{-1}$, which must hold for the continuous-media model to be valid. Therefore all electronic transitions induced by the acoustic waves are intravalley and the K- and K'-point spectra can still be considered separately using $\tau = \pm 1$.

Inserting Eqs. (2), (3), and (4) into Eq. (10) yields the Hamiltonian for an the electronic interaction with the acoustic Rayleigh waves as

$$\mathbf{H}_{\text{int}}^{\tau}\left(\mathbf{u}^{(q)}(x,y;t)\right) = u_0 e^{iqx-i\omega t}(iq)\Big\{g_1(T_1\mathbf{I}e^{-\lambda_l|q|y} + \\ +g_2\left(\left[-\tau T_2^{x,l}\boldsymbol{\sigma}_x + i\,\text{sgn}\,(q)T_2^{y}\boldsymbol{\sigma}_y\right]e^{-\lambda_l|q|y} + \right. \\ \left. +\left[\tau T_2^{x,t}\boldsymbol{\sigma}_x - i\,\text{sgn}\,(q)T_2^{y}\boldsymbol{\sigma}_y\right]e^{-\lambda_t|q|y}\right)\Big\} + \text{H.c.}, \qquad (11)$$

where the constants are

$$T_1 = 0.34,\ T_2^{y} = 1.6,\quad T_2^{x,l} = 1.7,\ T_2^{x,t} = 1.2\,. \qquad (12)$$

Considering the scaled spectra for the K- and K'-points in Fig. 2, we have, for a finite gate voltage V_G, that the scaled Fermi energy is

$$\tilde{E}^F \equiv \frac{E^F}{E_1} = -\alpha\frac{V_G[\text{V}]}{\sqrt{B\,[\text{T}]}}, \qquad (13)$$

where $V_G[\text{V}]$ is the gate voltage in volts and the proportionality factor is

$$\alpha = \frac{\sqrt{e}}{v^F\sqrt{2\hbar}}\,\text{V/T}^{1/2} \approx 1.4. \qquad (14)$$

This means the effect of tuning V_G *and/or* B is to simply shift the *scaled* Fermi level in the *scaled* spectrum. Doing so alters the number of dispersive energy bands crossing the Fermi level. If

$$|\tilde{E}_{n-1}| < |\tilde{E}^F| < |\tilde{E}_n|, \qquad (15)$$

where $\tilde{E}_n$ refers to the scaled energy of bulk Landau level n (see Eq. (8)), there will be n edge bands ($n-1$ edge bands) crossing the Fermi level in the K-spectrum (K'-spectrum). These crossings are the quantized conduction channels of the quantum Hall effect theory and the absolute values in Eq. (15) correspond to the electron–hole symmetry of the spectrum. The dispersionless level in the K'-spectrum never crosses the Fermi level and is therefore assumed never to be involved in transitions.

To analyze the possible electronic transitions we neglect back-scattering due to the assumed low amplitude of the acoustic wave and consider the transition rate between levels, thereby introducing conservation laws. The transition rate $W_{m,n}$ for an electronic jump from edge band n to edge band m due to interaction with an acoustic wave with scaled wave number $ql_B \equiv \tilde{q}$ is given by the Fermi golden rule,

$$W_{m,n} = \frac{2\pi}{\hbar}\sum_{\tilde{k}_n}\int d\tilde{E}_m\delta\left(\tilde{E}_n + \tilde{E}_R - \tilde{E}_m\right)\delta_{\tilde{k}_n+\tilde{q},\tilde{k}_m} \times \\ \times\rho(E_m)\left|\Lambda_{\tilde{k}_m;\tilde{q};\tilde{k}_n}^{\tau}\right|^2 f_{FD}(E_n)\left(1-f_{FD}(E_m)\right). \qquad (16)$$

Here, $\delta_{\tilde{k}_n+\tilde{q},\tilde{k}_m}\Lambda_{\tilde{k}_m;q;\tilde{k}_n}^{\tau}$ is the matrix element of a transition from $\tilde{k}_n$ to $\tilde{k}_m$, induced by an acoustic wave with wave number $\tilde{q}$. It is defined by

$$\delta_{\tilde{k}_n+\tilde{q},\tilde{k}_m}\Lambda^{\tau}_{\tilde{k}_m;\tilde{q};\tilde{k}_n} = l_B^2\iint \psi_\nu^{\tau,\tilde{k}_m\,\dagger}\mathbf{H}^{\tau}_{\rm int}(\mathbf{u}^{(q)})\psi_\nu^{\tau,\tilde{k}_n}d\tilde{x}d\tilde{y}, \tag{17}$$

where the interaction is given by Eq. (11) (the harmonic time dependence is accounted for by the energy conservation), the electronic wave functions are given in Appendix A and the integration surface is the whole sheet in terms of $(\tilde{x},\tilde{y})$. The continuous level index is $\nu = (E/E_1)^2$ as before, $f_{FD}(E(k))$ is the Fermi–Dirac distribution function, $\rho(E_m)$ is the density of final states, $\tilde{k}_n$ is the scaled wave number for an electronic state in edge band n corresponding to energy $\tilde{E}_n$, and the scaled acoustic dispersion is given by, using Eq. (6),

$$\tilde{E}_R(\tilde{q}) = \tilde{s}_R\,|\,\tilde{q}\,|, \tag{18}$$

with dimensionless speed of sound

$$\tilde{s}_R \equiv \frac{s_R}{\sqrt{2}v^F}. \tag{19}$$

The energy conservation and the Fermi–Dirac factors confine the energy region of absorption to the vicinity of the Fermi energy, $E_n \lesssim E^F \lesssim E_m$, and thus imply that the energies and wave numbers may be taken at the Fermi level, e.g., $\tilde{k}_n \to \tilde{k}_n^F$. Armed with this knowledge, the picture can be simplified by linearizing the spectrum, swapping each curved edge band n for a linear band n with velocity equal to the Fermi velocity v_n of the band, see Fig. 3. Then the linearized dimensionless dispersion of band n is

$$\tilde{E}_n(\tilde{k}_n) = \tilde{v}_n(\tilde{k}_n - \tilde{k}_n^F) + \tilde{E}^F, \tag{20}$$

where the dimensionless velocity of the band is defined analogously to Eq. (19),

$$\tilde{v}_n \equiv \frac{v_n}{\sqrt{2}v^F}, \tag{21}$$

and $\tilde{s}_R \ll \tilde{v}_n$.

The above arguments together with energy and momentum conservation restrict the number of allowed transitions by imposing the requirement that

$$\tilde{q} \approx \tilde{k}_m^F - \tilde{k}_n^F \equiv \Delta\tilde{k}_{m,n}^F, \tag{22}$$

i.e., the acoustic wave number $\tilde{q}$ must roughly match the $\tilde{k}$-separation of the two Fermi crossing points. Transitions occur in the vicinity of the Fermi level, so for the purpose of this calculation it is sufficient to take $\tilde{q} = \Delta\tilde{k}_{m,n}^F$. The same above arguments also imply that there are no allowed intra-level transitions, $n \neq m$.

The number of band-to-band transitions $N_t(n)$ for n Fermi level crossings is then

$$N_t(n) = \begin{cases} \dfrac{n!}{2(n-2)!} & \text{if } n \geq 2, \\ 0 & \text{if } n < 2, \end{cases} \tag{23}$$

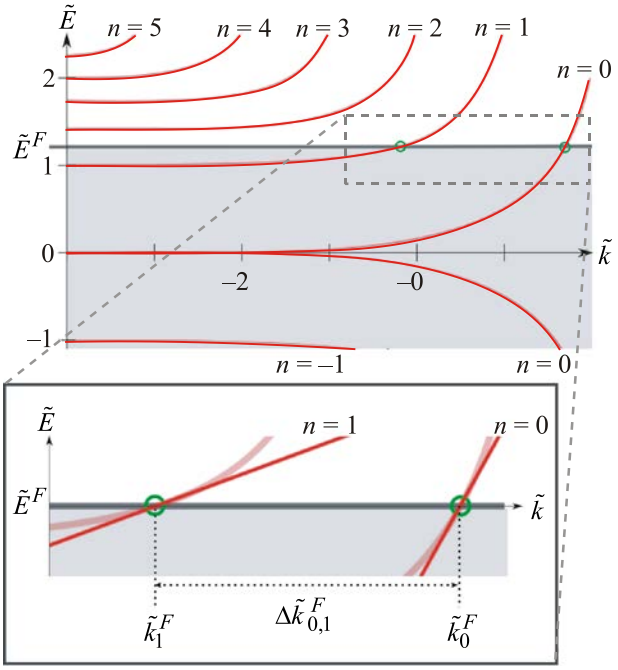

Fig. 3. (Color online) In the K-point spectrum of Fig. 2 the Fermi energy $\tilde{E}^F$ (horizontal grey line) is set by a gate voltage to lie between, say, bulk Landau level 1 and Landau level 2, thus giving the spectrum two Fermi crossing points (green circles), at $\tilde{k}_1^F$ and $\tilde{k}_0^F$, for edge band 1 and 0, respectively. Since transitions occur only near the Fermi level, the spectrum can be linearized, resulting in an effective model with two *linear* bands crossing the Fermi level at points $\tilde{k}_1^F$ and $\tilde{k}_0^F$ (see magnified inset). The resonant frequency is then given by the wave number separation at the Fermi level $\Delta\tilde{k}_{0,1}^F = |\,\tilde{k}_0^F - \tilde{k}_1^F\,|$. The picture is schematic.

and it must be remembered that transitions can occur in both the K- and K'-spectra.

Since the spacing $\Delta\tilde{k}_{n+1,n}^F$ between neighboring Fermi crossings is approximately equal for the same energy, i.e. $\Delta\tilde{k}_{n,n+j}^F \approx j\Delta\tilde{k}_{m,m+1}^F$, it is potentially useful to group the transitions in terms of how many bands they jump, i.e., a jump from band n to band $n-j$ is a j-jump (the minus sign is due to Fermi crossings of higher-n bands having lower $\tilde{k}$). For the situation with n Fermi crossings in one of the valley spectra, the number of j-jumps is

$$N_{t,j}(n) = \begin{cases} n-j & \text{if } n > 2, \\ 0 & \text{if } n \leq 2. \end{cases} \tag{24}$$

Summing $N_{t,j}$ for all $j < n$ yields the total number of transitions in the spectrum, N_t. Since all j-jumps have *approximately* equal $\Delta\tilde{k}_{m,n}^F$, i.e., absorbed acoustic frequency, they might appear as a multi-peak in the absorption spectrum: $N_{t,j}$ peaks close together.

The absorbed acoustic frequencies $sl_B^{-1}\Delta\tilde{k}_{m,n}^F$ can be found by using the electronic boundary conditions to find the Fermi level crossings $\tilde{k}_n^F$, see Appendix B. These frequencies are on the order of $sl_B^{-1} \sim \sqrt{B\,[\mathrm{T}]}\cdot 10^{11}\ \mathrm{s}^{-1}$ and

depend only on the scaled Fermi energy $\tilde{E}^F$. The periods of these acoustic frequencies must be much shorter than the acoustic decay time due to interaction with the electronic subsystem for the Fermi golden rule to remain valid.

For the linearized spectrum, Eq. (20), standard periodic boundary conditions in the x direction yields the density of final states per unit length $\rho(E_m)$ as

$$\rho(E_m) = \frac{1}{2\sqrt{2}\pi\hbar v^F \tilde{v}_m}. \tag{25}$$

As seen in Fig. 2, the density of states decreases with edge localization, i.e., increasing $\tilde{k}$ increases $\tilde{v}_n$. This effect decreases the strength of the absorption, but is not sufficient to counter the interaction since for Fermi levels in the range of the single-digit Landau levels, the edge bands typically have $\tilde{v}_n < 1$.

Since transitions occur near the Fermi level, the matrix element of transition in Eq. (17) is evaluated for $\tilde{q} = \Delta\tilde{k}_{m,n}$ and $\tilde{E}_n = \tilde{E}_m = \tilde{E}^F$, and is then

$$\Lambda^{\tau}_{\tilde{k}_m^F;\tilde{k}_n^F} = i\Delta\tilde{k}^F_{m,n}\left(\frac{u_0}{l_B}\right)\left(g_1F_1 + g_2F_2\right), \tag{26}$$

where the dimensionless transition-dependent integrals have been separated into a scalar potential contribution F_1 and pseudo-vector-potential contribution F_2; both given in Appendix C. Normalization of the electronic wave functions causes these integrals to be at the most unity.

Inserting the above into Eq. (16), the final expression for the absorption rate per unit length is

$$W_{m,n} = \left(\frac{1}{\sqrt{2}\hbar^2 v^F}\right)\frac{(\Delta\tilde{k}^F_{m,n})^2}{|\tilde{v}_m - \tilde{v}_n|}\left(\frac{u_0}{l_B}\right)^2 \left|g_1F_1 + g_2F_2\right|^2. \tag{27}$$

The first factor $\approx 1.6\cdot10^{24}\ \mathrm{eV^{-2}\cdot s^{-1}\cdot m^{-1}}$ and consists of general constants, and the second factor consists of parameters specific to the transition in question. The third is the amplitude dependence, with the amplitude scaled by the magnetic length. By assumption, the amplitude is low, causing this factor to be very small. The final factor is the coupling coefficients and the transition integrals, which are less than one by normalization, meaning that the order of magnitude is set by the coupling. Inserting the definition of the magnetic length yields $W_{m,n} \propto B$. This direct proportionality to the field comes from the x-derivatives in the strain tensor yielding a factor (iq) and the fact that absorption occurs only for the acoustic wave numbers q which match the electro-magnetic spectrum and thus are of the order of inverse magnetic length.

The total energy of the acoustic wave is [28]

$$E_{\mathrm{ac}} = \rho_{\mathrm{gr}}\omega(q)^2 \iint\limits_S |\mathbf{u}^{(q)}(x,y;0)|^2\, dxdy, \tag{28}$$

where $\rho_{\mathrm{gr}} = 7.6\cdot10^{-7}\ \mathrm{kg/m^2}$ is the surface mass density of graphene [19]. In this case

$$\iint\limits_S |\mathbf{u}^{(q)}(x,y;0)|^2\, dxdy = \frac{2Lu_0^2}{|q|N_{\mathrm{ac}}^2}, \tag{29}$$

and integration yields

$$N_{\mathrm{ac}} = 1.2, \tag{30}$$

whereas the energy lost to each electronic transition is simply $\hbar\omega(q)$. The inverse acoustic decay time τ_D due to interaction with the electronic subsystem is then given by

$$\frac{1}{\tau_D} = \left(\frac{N_{\mathrm{ac}}^2(\Delta\tilde{k}^F_{m,n})^2}{2\sqrt{2}\hbar v^F\,|\tilde{v}_m - \tilde{v}_n|\,\rho_{\mathrm{gr}}l_B^2 s_R}\right)\left|g_1F_1 + g_2F_2\right|^2 =$$

$$= \frac{2.0\cdot10^7\,B\,[\mathrm{T}]}{[\mathrm{s\cdot eV^2}]}\frac{(\Delta\tilde{k}^F_{m,n})^2}{|\tilde{v}_m - \tilde{v}_n|}\left|g_1F_1 + g_2F_2\right|^2. \tag{31}$$

As an example, consider the simplest case. The gate voltage is adjusted in relation the magnetic field so that

$$\tilde{E}^F = \frac{\tilde{E}_1 + \tilde{E}_2}{2}, \tag{32}$$

i.e., the Fermi level is now in the middle of the gap between Landau level 1 and 2. According to Eq. (15), there will be 2 bands crossing the Fermi level in the K-point spectrum (1 in the K'-spectrum) and by Eq. (23) there will, trivially, be 1 possible transition (0 possible transitions). Equation (24) specifies that this one transition will be between neighboring edge bands. Solving Eq. (B.1) numerically returns $\tilde{k}_1^F = -1.29$ and $\tilde{k}_0^F = 0.36$, the points where the bands intersect the Fermi level. This leads to $\Delta\tilde{k}^F_{0,1} = 1.65$, which will be the acoustic wave number absorbed in the transition from edge band 1 to edge band 0. The fixed $\tilde{E}^F$ means that the generalized level index is, according to Eq. (B.3), $\nu^F = ((1+\sqrt{2})/2)^2 \approx 1.4571$ and the band velocities are estimated to $\tilde{v}_0 \approx 0.6$ and $\tilde{v}_1 \approx 0.3$. Using the wave functions of Eq. (A.2) with parameters ν^F and $\tilde{k}_1^F$ ($\tilde{k}_0^F$) for edge band 1 (0) as well as the acoustic wave number $\Delta\tilde{k}^F_{0,1}$ allows for numerical evaluation of the integrals in Appendix C. The interaction integrals in Eqs. (C.1) and (C.2) yield $F_1 = -0.0546$ and $F_2^{\tau} = -0.0918$. Inserting all known values into Eq. (31) the resulting inverse decay time is

$$\frac{1}{\tau_D} = \frac{1.8\cdot10^8\,B\,[T]}{[\mathrm{s\cdot eV^2}]}\left|0.0546g_1 + 0.0918g_2\right|^2. \tag{33}$$

With the standard values [27] of $g_1 \approx 20$ eV and $g_2 \approx 2$ eV, the decay time becomes $\tau_D \approx 3.4\ \mathrm{ns}/B\,[\mathrm{T}]$, which corresponds to a characteristic decay length of $41\ \mu\mathrm{m}/B\,[\mathrm{T}]$. For reasonable magnetic fields, the decay time is much longer than the acoustic period $\sim\sqrt{B\,[\mathrm{T}]}\,10^{-11}$ s, thus validating our use of the Fermi golden rule. The prerequisite for this transition, Eq. (32), together with Eqs. (13) and (14), means

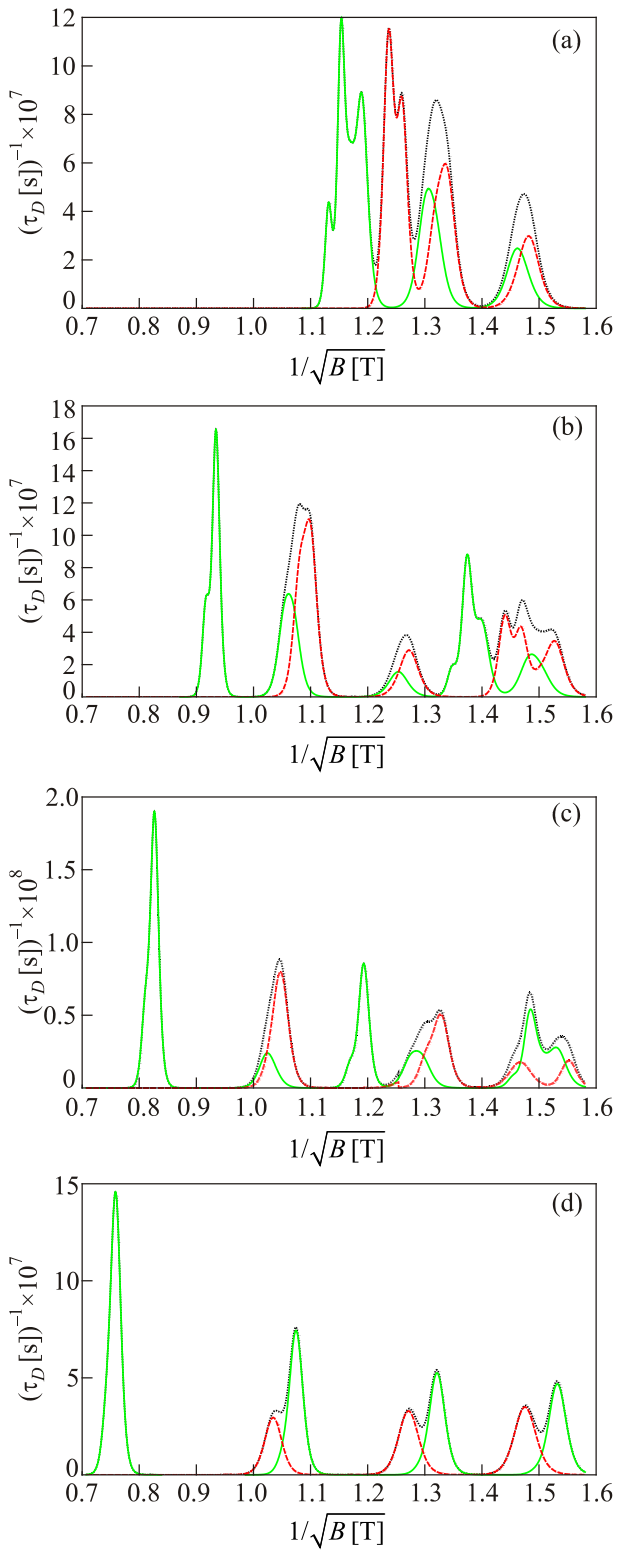

Fig. 4. (Color online) Inverse acoustic decay time in seconds $\tau_D\,[\mathrm{s}]^{-1}$ vs inverse square root of magnetic field in Tesla $1/\sqrt{B\,[\mathrm{T}]}$ for gate voltage $V_G = -50$ mV and temperature $T = 5$ K, calculated for acoustic ordinary frequencies (a) $f_{\mathrm{ac}} = 0.85\cdot 10^{11}\ \mathrm{s}^{-1}$, (b) $f_{\mathrm{ac}} = 1.25\cdot 10^{11}\ \mathrm{s}^{-1}$, (c) $f_{\mathrm{ac}} = 1.65\cdot 10^{11}\ \mathrm{s}^{-1}$, (d) $f_{\mathrm{ac}} = 2.20\cdot 10^{11}\ \mathrm{s}^{-1}$. Absorption due to electronic transitions in the K-valley (K'-valley) is given by the solid green (dashed red) line. The total absorption, summed over both valleys, is given by the dotted black line (partially obscured).

that the transition requires $-V_G\,[\mathrm{V}]/\sqrt{B\,[\mathrm{T}]} \sim 1$. In addition, the acoustic frequency must be such that its scaled wavenumber, which is dependent on the magnetic field, fulfills $\tilde{q} \approx \Delta\tilde{k}^F = 1.65$.

In order to study the electronic absorption as a function of magnetic field, we performed a numerical simulation and plotted the inverse acoustic decay time of Eq. (31) vs $1/\sqrt{B\,[\mathrm{T}]}$ with a fixed gate voltage $V_G = -50$ mV for different acoustic frequencies $\omega = 2\pi f_{\mathrm{ac}}$. By decreasing the magnetic field, the effective Fermi level is shifted upward in the scaled spectrum of Fig. 2; simultaneously, the acoustic wave number is continuously being rescaled according to $\tilde{q} = ql_B$. Valleys K and K' are treated separately, but both contribute to the total absorption. In the numerical model we introduced a finite electronic relaxation time $\tau_{\mathrm{el}} \sim 10^{-10}$ s and a small temperature $T = 5$ K.

The resulting absorption plots are shown in Fig. 4 and the corresponding resonant transitions are plotted in the scaled electronic spectrum in Fig. 5. As shown, for a given acoustic frequency propagation may be blocked for several values of the magnetic field due to multiple resonant transitions, but for a given pair of edge bands n and m, resonance occurs only for a certain continuous interval of B. Generally, it can be shown that transitions n to m occur when

$$\Delta\tilde{k}^F_{mn} < \tilde{q} < \frac{\tilde{v}_m}{\tilde{v}_n}\Delta\tilde{k}^F_{mn}. \qquad (34)$$

In conclusion, we have demonstrated that a stress-free graphene edge supports propagating vibrational in-plane edge modes in the form of 2D Rayleigh waves, and that interaction with such waves can cause electronic transitions between the electronic edge states induced by a perpendicular magnetic field. Since momentum conservation requires the wavelength of the acoustic waves to be on the scale of the magnetic length for transitions to occur, the magnetic field strength enters into the matrix element as a simple proportionality through the strain tensor. Finally we studied the acoustic decay time as a function of magnetic field strength for several acoustic frequencies, and found that for a given acoustic frequency the medium can become non-transparent for several values of the magnetic field, corresponding to different resonant transitions. The results could be verified by, e.g., tuning the magnetic field for a fixed gate voltage while measuring the decay of propagating acoustic edge waves. We suggest, based on comparison with similar systems [29], that this edge-localized interaction could result in nonlinear phenomena such as acoustic solitons propagating along the edge. Such solitons will be the subject of a future paper.

Acknowledgements

We would like to thank L. Gorelik for valuable discussion, E. Cojocaru [30], J. Schwizer [31] and B. Shoelson [32] for their Matlab scripts and the Swedish Research Council (VR) for funding.

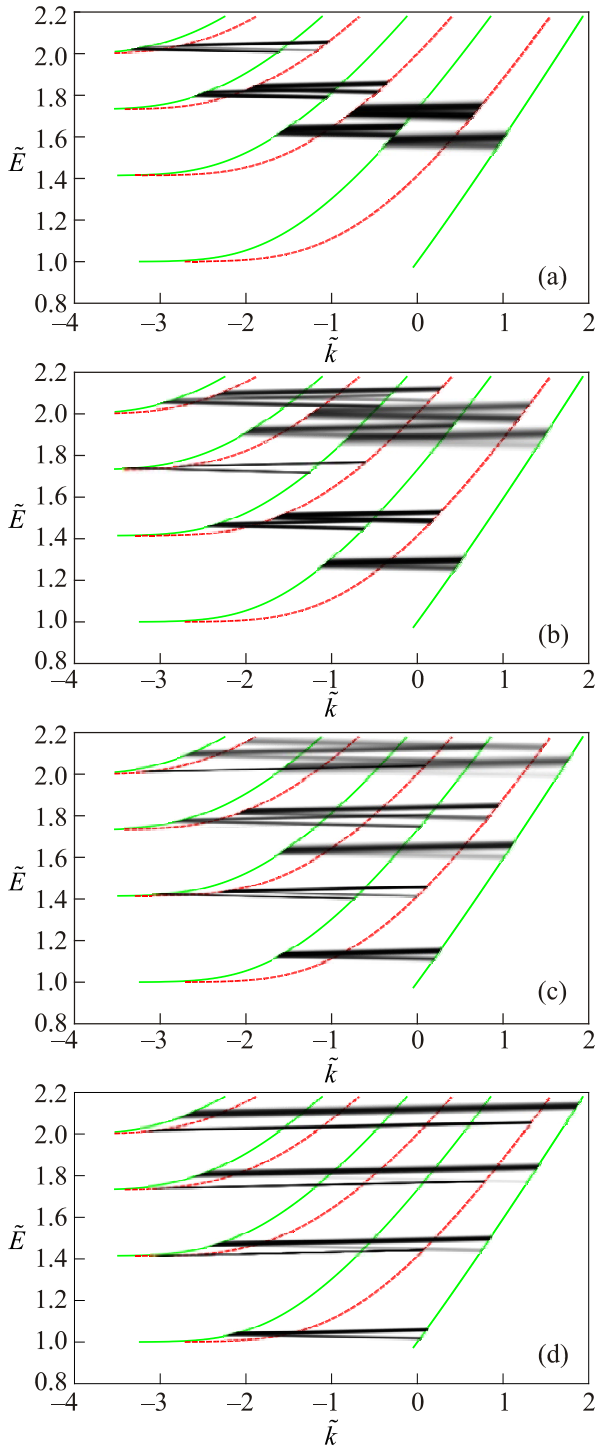

Fig. 5. (Color online) The transitions corresponding to the absorption peaks in Fig. 4 shown as black lines in the scaled energy spectrum. The K-valley (K'-valley) spectrum is given by the solid green (dashed red) lines and the transition line opacity is proportional to the (relative) inverse decay time of the associated transition. The figures are for the acoustic ordinary frequencies (a) $f_{ac} = 0.85 \cdot 10^{11}\ \mathrm{s}^{-1}$, (b) $f_{ac} = 1.25 \cdot 10^{11}\ \mathrm{s}^{-1}$, (c) $f_{ac} = 1.65 \cdot 10^{11}\ \mathrm{s}^{-1}$, and (d) $f_{ac} = 2.20 \cdot 10^{11}\ \mathrm{s}^{-1}$, with gate voltage $V_G = -50$ mV and temperature $T = 5$ K.

Appendix A: Electronic wave functions

The electronic pseudospinor wave functions, labeled by valley index τ, wave number $\tilde{k}$, and continuous level index ν, are [12–15]

$$\psi_\nu^{\tau,\tilde{k}}(x,y) = \frac{N_\nu^{\tau,\tilde{k}}}{\sqrt{Ll_B}} e^{i\tilde{k}\tilde{x}} \phi_\nu^{\tau,\tilde{k}}(\tilde{y}), \tag{A.1}$$

where τ labels the valley (K or K') as before. The y-dependent factor is

$$\phi_\nu^{+1,\tilde{k}}(\tilde{y}) = \begin{pmatrix} D_\nu(\sqrt{2}(\tilde{k}+\tilde{y})) \\ \sqrt{\nu} D_{\nu-1}(\sqrt{2}(\tilde{k}+\tilde{y})) \end{pmatrix}, \tag{A.2}$$

for the K-point and

$$\phi_\nu^{-1,\tilde{k}}(\tilde{y}) = \begin{pmatrix} \sqrt{\nu} D_{\nu-1}(\sqrt{2}(\tilde{k}+\tilde{y})) \\ D_\nu(\sqrt{2}(\tilde{k}+\tilde{y})) \end{pmatrix}, \tag{A.3}$$

for the K'-point. The factors $N_\nu^{\tau,k} / \sqrt{Ll_B}$ are normalization constants, see Eq. (C.3).

Appendix B: Fermi level crossings

The edge boundary condition of Eq. (9) ultimately gives an equation for the electronic spectrum. At the Fermi energy E^F this equation reads for the K-point

$$D_{\nu^F}(\sqrt{2}\tilde{k}^F) = 0, \tag{B.1}$$

and for the K'-point

$$D_{\nu^F-1}(\sqrt{2}\tilde{k}^F) = 0, \tag{B.2}$$

where

$$\nu^F = (\tilde{E}^F)^2. \tag{B.3}$$

Solving Eqs. (B.1) and (B.2) for $\tilde{k}^F$ gives the Fermi crossing points $\tilde{k}_n^F$ for the given $\tilde{E}^F$. Identifying them with the different bands allows for calculation of $\Delta\tilde{k}_{m,n}^F$ and thus the absorbed acoustic frequencies. In general $\Delta\tilde{k}_{m,n}^F \sim 1$.

Appendix C: Absorption integrals

Here the dimensionless transition integrals that enter into the transition matrix element are given. Since the integrands decay into the bulk, they are easily evaluated using a cutoff. The integral giving the scalar-potential contribution to the absorption is (normalization constants have been moved to the left hand side for brevity)

$$\frac{F_1}{N_{\nu^F}^{\tau,\tilde{k}_m^F *} N_{\nu^F}^{\tau,\tilde{k}_n^F}} = T_1 \int_0^\infty \phi_{\nu^F}^{\tau,\tilde{k}_m^F \dagger}(\tilde{y}) \phi_{\nu^F}^{\tau,\tilde{k}_n^F}(\tilde{y}) e^{-\lambda_l |\Delta\tilde{k}_{m,n}^F| \tilde{y}} d\tilde{y}, \tag{C.1}$$

and the pseudo-vector-potential contribution integral is

$$\frac{F_2}{N_{\nu^F}^{\tau,\tilde{k}_m^F *} N_{\nu^F}^{\tau,\tilde{k}_n^F}} = \tau \int_0^\infty \phi_{\nu^F}^{\tau,\tilde{k}_m^F \dagger}(\tilde{y}) \sigma_x \phi_{\nu^F}^{\tau,\tilde{k}_n^F}(\tilde{y}) \times$$
$$\times \left(-T_2^{x,l} \mathrm{e}^{-\lambda_l \Delta |\tilde{k}_{m,n}^F| \tilde{y}} + T_2^{x,t} \mathrm{e}^{-\lambda_t |\Delta \tilde{k}_{m,n}^F| \tilde{y}} \right) d\tilde{y} +$$
$$+ i \, \mathrm{sgn}\,(\Delta \tilde{k}_{m,n}^F) T_2^y \int_0^\infty \phi_{\nu^F}^{\tau,\tilde{k}_m^F \dagger}(\tilde{y}) \sigma_y \phi_{\nu^F}^{\tau,\tilde{k}_n^F}(\tilde{y}) \times$$
$$\times \left(\mathrm{e}^{-\lambda_l \Delta |\tilde{k}_{m,n}^F| \tilde{y}} - \mathrm{e}^{-\lambda_t |\Delta \tilde{k}_{m,n}^F| \tilde{y}} \right) d\tilde{y}. \qquad \text{(C.2)}$$

The numerical normalization constants are given by

$$\left| N_{\nu^F}^{\tau,\tilde{k}_n^F} \right|^2 = \frac{1}{\int_0^\infty \left| \phi_{\nu^F}^{\tau,\tilde{k}_n^F}(\tilde{y}) \right|^2 d\tilde{y}}. \qquad \text{(C.3)}$$

1. K.S. Novoselov, A.K. Geim, S.V. Morozov, D. Jiang, Y. Zhang, S.V. Dubonos, I.V. Grigorieva, and A.A. Firsov, *Science* **306**, 666 (2004).
2. A.K. Geim and K.S. Novoselov, *Nat. Mater.* **6**, 183 (2007).
3. L.D. Landau and E.M. Lifshitz, *Theory of Elasticity*, Butterworth-Heinemann, Oxford (2008).
4. J. Heil, I. Kouroudis, B. Luthi, and P. Thalmeier, *J. Phys. C*: *Solid State Physics* **17**, 2433 (1984).
5. R.L. Willett, P.A. Maksym, and T. Chakraborty, *Phys. Rev. Lett.* **65**, 112 (1990).
6. R.L. Willett, R.R. Ruel, M.A. Paalanen, K.W. West, and L.N. Pfeiffer, *Phys. Rev. B* **47**, 7344 (1993).
7. P. Thalmeier, *Phys. Rev. B* **83**, 125314 (2011).
8. S.H. Simon, *Phys. Rev. B* **54**, 13878 (1996).
9. P. Thalmeier, B. Dóra, and K. Ziegler, *Phys. Rev. B* **81**, 041409 (2010).
10. A.V. Savin and Y.S. Kivshar, *Phys. Rev. B* **81**, 165418 (2010).
11. N.M.R. Peres, F. Guinea, and A.H. Castro Neto, *Phys. Rev. B* **73**, 125411 (2006).
12. V.P. Gusynin, V.A. Miransky, S.G. Sharapov, and I.A. Shovkovy, *Fiz. Nizk. Temp.* **34**, 993 (2008) [*Low Temp. Phys.* **34**, 778 (2008)].
13. V.P. Gusynin, V.A. Miransky, S.G. Sharapov, and I.A. Shovkovy, *Phys. Rev. B* **77**, 205409 (2008).
14. V.P. Gusynin, V.A. Miransky, S.G. Sharapov, I.A. Shovkovy, and C.M. Wyenberg, *Phys. Rev. B* **79**, 115431 (2009).
15. I. Romanovsky, C. Yannouleas, and U. Landman, *Phys. Rev. B* **83**, 045421 (2011).
16. A.H. Castro Neto, F. Guinea, N.M.R. Peres, K.S. Novoselov, and A.K. Geim, *Rev. Mod. Phys.* **81**, 109 (2009).
17. L. Brey and H.A. Fertig, *Phys. Rev. B* **73**, 195408 (2006).
18. E.V. Castro, H. Ochoa, M.I. Katsnelson, R.V. Gorbachev, D.C. Elias, K.S. Novoselov, A.K. Geim, and F. Guinea, *Phys. Rev. Lett.* **105**, 266601 (2010).
19. K. Kaasbjerg, K.S. Thygesen, and K.W. Jacobsen, *Phys. Rev. B* **85**, 165440 (2012).
20. K. Nakada, M. Fujita, G. Dresselhaus, and M.S. Dresselhaus, *Phys. Rev. B* **54**, 17954 (1996).
21. K.S. Novoselov, A.K. Geim, S.V. Morozov, D. Jiang, M.I. Katsnelson, I.V. Grigorieva, S.V. Dubonos, and A.A. Firsov, *Nature* **438**, 197 (2005).
22. Z. Jiang, E.A. Henriksen, L.C. Tung, Y.-J. Wang, M.E. Schwartz, M.Y. Han, P. Kim, and H.L. Stormer, *Phys. Rev. Lett.* **98**, 197403 (2007).
23. G. Li, E.Y. Andrei, and A.A. Firsov, *Nat. Phys.* **3**, 623 (2007).
24. L. Brey and H.A. Fertig, *Phys. Rev. B* **73**, 235411 (2006).
25. M. Fujita, K. Wakabayashi, K. Nakada, and K. Kusakabe, *J. Phys. Soc. Jpn.* **65**, 1920 (1996).
26. M. Arikawa, Y. Hatsugai, and H. Aoki, *Phys. Rev. B* **78**, 205401 (2008).
27. H. Suzuura and T. Ando, *Phys. Rev. B* **65**, 235412 (2002).
28. H. Ezawa, *Ann. Phys.* **67**, 438 (1971).
29. A.E. Borovik, E.N. Bratus, and V.S. Shumeiko, *Sov. Phys. JETP* **68**, 826 (1989).
30. E. Cojocaru, *arXiv:0901.**2220**, Mathworks online database* (2009). URL: *http://www.mathworks.se/matlabcentral/fileexchange/22620*.
31. J. Schwizer, *Mathworks online database* (2005). URL: *http://www.mathworks.com/matlabcentral/fileexchange/7401*.
32. B. Shoelson, *Mathworks online database* (2012). URL: *http://www.mathworks.com/matlabcentral/fileexchange/36953.*